FORUM GEOGRAFI
ISSN: 0852-0682 | E-ISSN: 2460-3945

HTTPS://JOURNALS.UMS.AC.ID/INDEX.PHP/FG/

Research article

Assessing Landslide Susceptibility in Batu City, Indonesia: A Machine Learning Approach Using Google Earth Engine

Muhardi[1,3], Adi Susilo[1,4*], Eko Andi Suryo[2], Yoga Satria Putra[3], Muwardi Sutasoma[1], Rahmat Faizal[1,5], Nur Aini Gama Lestari[1], Rony Prianto Nugraha[6], Andy Anderson Bery[7], Muhammad Fathur Rouf Hasan[4,8]

[1] Department of Physics, Universitas Brawijaya, Malang 65145, Indonesia; [2] Department of Civil Engineering, Universitas Brawijaya, Malang 65145, Indonesia; [3] Geophysics Study Program, Universitas Tanjungpura, Pontianak 78124, Indonesia; [4] Study Center for Geosciences and Hazard Mitigation, Universitas Brawijaya, Malang 65145, Indonesia; [5] Department of Civil Engineering, Universitas Borneo Tarakan, Tarakan 77123, Indonesia; [6] Department of Engineering Science, The University of Auckland, Private Bag, Auckland 90210, New Zealand; [7] Earth System Processes and Hazard Modeling Center, Geophysics Programme, School of Physics, Universiti Sains Malaysia, Penang 11800, Malaysia; [8] Graduate School, Universitas Brawijaya, Malang 65145, Indonesia.

[*)] Correspondence: adisusilo@ub.ac.id

Citation:
Muhardi, Susilo, A., Suryo, E. A., Putra, Y. S., Sutasoma, M., Faizal, R., Lestari, N. A. G., Nugraha, R. P., Bery, A. A., & Hasan, M. F. R. (2026). Assessing Landslide Susceptibility in Batu City, Indonesia: A Machine Learning Approach Using Google Earth Engine. *Forum Geografi*. 40(2), 260-276.

Article history:
Received: 24 March 2026
Revised: 26 May 2026
Accepted: 9 June 2026
Published: 10 June 2026

Abstract

This study aims to map landslide susceptibility in Batu City, East Java Province, Indonesia, using machine learning on the Google Earth Engine platform. Five algorithms were used: random forest (RF), classification and regression trees, support vector machine, gradient tree boosting, and *k*-nearest neighbors. Landslide susceptibility data were collected from 276 sample points, comprising 138 landslides and 138 nonlandslides. The data were divided into two parts: 70% for training and 30% for testing. The conditioning factors initially considered consisted of 13 variables. Pearson correlation matrix analysis indicated that annual rainfall should be excluded to avoid multicollinearity, resulting in 12 predictors used for mapping: elevation, slope, aspect, landforms, distance from rivers, topographic wetness index, soil types, land use/land cover, normalized difference vegetation index, distance from roads, geological formations, and distance from lineaments. Model performance was evaluated using six metrics: accuracy, precision, recall (sensitivity), F1-score, kappa coefficient, and area under the receiver operating characteristic curve. Model validation results indicated that the RF algorithm was the best model. The RF-based landslide susceptibility map classified the area into five classes: very low class covering an area of 60.70 km^2 (30.49%), low class covering an area of 29.47 km^2 (14.80%), medium class covering an area of 16.21 km^2 (8.14%), high class covering an area of 22.56 km^2 (11.33%), and very high class covering an area of 70.16 km^2 (35.24%). Variable importance analysis showed that slope is the most influential factor, with a mean decrease in impurity of 43.77 (15.36%), whereas soil types had the least contribution. This study successfully mapped landslide susceptibility using a machine learning approach, enabling direct support for disaster mitigation planning and risk-based land use in Batu City.

Keywords: Google Earth Engine; Landslide Susceptibility Map; Machine Learning; Random Forest.

1. Introduction

Landslides are among the most destructive natural disasters worldwide. Between 1903 and 2023, they caused 73,278 deaths and left more than 15 million people injured or homeless globally (Ayala, 2025). In developing countries, anthropogenic activities, such as deforestation, infrastructure development, and land-use changes, can significantly accelerate landslide occurrence (Huang *et al.,* 2020). Large-scale deforestation and uncontrolled urbanization indirectly remove slope-stabilizing vegetation and disrupt natural drainage systems (Ayala, 2025). Additionally, natural factors, such as extreme rainfall, seismic activity, and volcanic activity, can serve as primary natural triggers (Highland & Bobrowsky, 2008). In Indonesia, landslides are among the most frequent hydrogeomorphic disasters. According to recorded data from 514 regencies, 224 (43.58%) are classified as high risk, 224 (43.58%) as moderate risk, and 66 (12.84%) as low risk for landslides (Bagaskoro *et al.,* 2025). Complex topographic conditions and high volcanic activity create dynamic interactions among triggering factors that increase susceptibility. This is particularly relevant in steep mountain ranges composed of unconsolidated young volcanic rock, such as those found across much of the island of Java (Noviyanto *et al.,* 2020; Susilo *et al.,* 2023). Additional primary triggers include extreme rainfall, weathered lithology, land-use changes, and development activities that disrupt slope stability (Nurwatik *et al.,* 2022). Global climate change can also intensify extreme rainfall, which can directly trigger slope instability (Ayala, 2025). Therefore, understanding the systemic relationships between global change and landslides has become acutely urgent. A holistic approach integrating land-use planning, disaster mitigation, and climate change adaptation is needed to reduce the risk of future landslides.

Mapping landslide susceptibility is essential in land-use planning for identifying areas at risk of slope failure. This effort also helps reduce disaster risk, guide land-use planning, protect

infrastructure, and implement mitigation strategies (Huang *et al.,* 2020; Zhou *et al.,* 2024). Thus, accurate and reliable maps are needed by governments as policymakers to prioritize high-risk zones for intervention, regulate development in vulnerable areas, and design early warning systems (Suwarno e*t al.,* 2025). Without map-based planning, disaster mitigation efforts tend to be reactive, leading to losses that could otherwise be anticipated and prevented (Hou *et al.,* 2025). The maps can also provide information on areas unsuitable for construction and those requiring engineering measures, such as retaining walls or drainage systems (Asmare *et al.,* 2023). In addition, early warning systems can be calibrated using susceptibility zones. For example, in evacuation warnings, areas with very high landslide susceptibility may require lower rainfall thresholds than those with low landslide susceptibility (Hasan *et al.,* 2024). In Indonesia, decentralization has granted regencies greater authority in regional spatial planning, making locally relevant susceptibility maps urgently needed (Suwarno *et al.,* 2025). However, many local governments still rely on conventional mapping approaches because of their limited technical capacity or computational resources. Therefore, developing an accessible cloud-based workflow that produces reliable, regularly updated landslide susceptibility maps is a crucial step toward prioritizing disaster risk reduction within regional development planning processes (Prasetyo *et al.,* 2025).

One of the most comprehensive methods for mapping landslide susceptibility is machine learning (Hussain *et al.,* 2023; Chen, 2025). It can process and integrate continuous, categorical, raster, and vector data, making them highly relevant for complex geospatial modeling (Ersayin & Uzun, 2025; Liu, 2024). In contrast, conventional methods are often limited by their assumption of linear relationships between variables that cause landslides (Huang *et al.,* 2020). Consequently, susceptibility mapping has increasingly shifted to machine learning methods, which are data-driven and more adaptive to complex, nonlinear variable relationships (Liu *et al.,* 2022). Several commonly used machine learning algorithms, such as random forest (RF), classification and regression trees (CART), gradient tree boosting (GTB), support vector machine (SVM), and k-nearest neighbors (KNN), can extract patterns from various geospatial data and produce probabilistic predictions with excellent accuracy (Zhou *et al.,* 2024; Kavzoglu & Teke, 2022; Anuragi, 2025; Liu *et al.,* 2022; Ali *et al.,* 2024). Decision-tree-based machine learning algorithms can handle large datasets, detect interactions among variables, and quantify the influence of each factor through feature importance (Chen, 2025; Liu *et al.,* 2022). Among these methods, RF is highly robust to outliers and data noise, CART can handle both numerical and categorical features without requiring special normalization, and GTB can improve models through iterative boosting, thereby increasing prediction accuracy (Fu *et al.,* 2025; Kavzoglu & Teke, 2022). In addition to tree-based algorithms, other algorithms used in this study are SVM and KNN. SVM effectively detects nonlinear class boundaries using kernel functions, whereas KNN offers a simple distance-based approach that is powerful at recognizing local patterns (Anuragi, 2025; Li *et al.,* 2025). Comparing these algorithms enables the identification of the model with the best overall algorithmic performance for landslide susceptibility prediction.

Studies that systematically implement and compare various machine learning algorithms within the Google Earth Engine (GEE) cloud computing platform for landslide susceptibility mapping in tropical volcanic regions, particularly in Indonesia, remain very limited. Although previous studies have applied various machine learning algorithms for landslide susceptibility mapping, most relied on desktop-based workflows that require manual integration of diverse data sources and significant local computational resources. This poses a challenge in tropical regions such as Indonesia, where high rainfall intensity and complex geomorphological features, including steep slopes on poorly consolidated pyroclastic material, increase landslide susceptibility (Tjahjono *et al.,* 2024; Noviyanto *et al.,* 2020). Furthermore, conventional vector-based approaches are less suitable for updating temporal information, making raster- and cloud-based approaches more reliable for landslide hazard modeling (Tjahjono *et al.,* 2024). Although previous studies have compared the performances of machine learning algorithms, comparative assessments with balanced landslide and nonlandslide sample designs, coupled with explicit variable importance analysis adapted for spatial planning purposes, remain scarce in Indonesia's young volcanic landscapes. This study directly addresses this gap by implementing a fully reproducible, scalable cloud-native workflow using GEE, thereby eliminating reliance on high-performance local computing infrastructure. Thus, this study not only produces accurate landslide susceptibility maps but also provides a methodological framework that can be adopted by stakeholders in other landslide-prone regions of Indonesia.

Batu City, East Java Province, is one of Indonesia's landslide-prone regions. This is due to its undulating topography, with steep mountain slopes dominated by volcanic material. In addition, tourism development and land-use change in some areas have contributed to decreased slope

stability (Noviari *et al.,* 2023; Tjahjono *et al.,* 2024). Its geomorphological conditions are also quite complex because it is located on the volcanic slopes of Arjuno–Welirang (Agung *et al.,* 2023). The subsurface geological formations are also unique, consisting of breccia, tuff, and young volcanic rocks, resulting in a high degree of weathering. This makes the subsurface layer prone to erosion (Susilo *et al.,* 2023). In addition, the average annual rainfall is relatively high, which can trigger landslides (Hasan *et al.,* 2024). These conditions make Batu City an appropriate case study for mapping and developing landslide susceptibility models, especially in tropical volcanic regions (Pratiwi *et al.,* 2024). Specifically, Batu City exhibits the full range of characteristics that characterize high landslide risk in tropical volcanic environments: steep volcanic terrain underlain by poorly consolidated pyroclastic deposits, rapid land-use conversion driven by tourism, and high seasonal rainfall that frequently triggers slope failures (Noviyanto *et al.,* 2020; Susilo *et al.,* 2023). Therefore, this region is an ideal location for developing and testing landslide-susceptibility models using machine learning. The results obtained can be directly applied to other volcanic regions in Indonesia and surrounding areas facing similar hazard risks.

This study contributes to the literature by developing a reproducible machine-learning framework in the GEE platform to assess landslide susceptibility using integrated topographic, hydrological, vegetative, rainfall, and land-use factors. The main novelty of this study lies in the combination of three factors that are rarely found together in landslide studies in Indonesia, particularly in the Batu City area. First, this study combines landslide conditioning factors and processes them using GEE. This cloud-based platform enables parallel processing of multisource data, thereby overcoming the limitations of conventional computing. Second, this study implements and compares five algorithms (RF, CART, GTB, SVM, and KNN) using a robust validation scheme in an area with complex young volcanic characteristics. Third, this study explicitly addresses the identification of the best algorithm when trigger factor data have heterogeneous resolutions and types using a balanced distribution of landslide and nonlandslide sample points. By presenting a variable importance analysis of the best model, it provides a physical interpretation that can be directly utilized in risk-based spatial planning. Specifically, it applies the proposed framework to an area within the young volcanic complex of Arjuno–Welirang, which is characterized by steep slopes, poorly consolidated pyroclastic material, high rainfall, and land-use changes driven by tourism—factors that increase landslide risk. Thus, this study's contribution is not only the production of a landslide susceptibility map for Batu City but also the provision of a measurable and replicable workflow for other landslide-prone areas in Indonesia.

This study aims to assess landslide susceptibility in Batu City, East Java Province, Indonesia, using machine learning on the GEE platform. More specifically, this study pursues the following specific objectives: (1) to produce a landslide susceptibility map using five machine learning algorithms based on condition factors derived from open-access remote sensing and geospatial data; (2) to validate and compare model performance using various evaluation metrics to identify the most reliable algorithm for the study area (Hou *et al.,* 2025); (3) to analyze the importance of variables from the best-performing model to determine which factors most strongly influence landslide occurrence. Previous studies have shown that topographic conditions (e.g., slope and elevation), geomorphological characteristics (e.g., landforms), hydrological factors (e.g., river density and rainfall intensity), land surface factors (e.g., soil type, vegetation indices, and land use), anthropogenic factors (e.g., road density), and geological formations all influence slope stability (Heo *et al.,* 2024; Arabameri *et al.,* 2020; Asmare *et al.,* 2023; Pasang & Kubíček, 2020); and (4) to demonstrate a fully reproducible cloud-native workflow that can be transferred to other landslide-prone regions in Indonesia and surrounding areas, thereby reducing technical barriers to disaster risk reduction. By achieving these objectives, this study not only produces practical, high-resolution susceptibility maps for Batu City but also provides a scalable methodological template, thereby contributing to disaster mitigation.

2. Methods

This study consists of three stages: data preparation, data processing and modeling, and model validation (Figure 1). The landslide susceptibility mapping process began with the preparation of 13 variable maps: elevation, slope, aspect, landforms, annual rainfall, distance from rivers, topographic wetness index (TWI), soil types, land use/land cover (LULC), normalized difference vegetation index (NDVI), distance from roads, geological formations, and distance from lineaments. They were then combined into multiband raster data and subjected to multicollinearity testing. An inventory of landslide distribution data, consisting of landslide and nonlandslide points, was compiled. Active landslide points were labelled 1, whereas nonlandslide points were labelled 0. In data processing and modeling, the data were split into 70% for training and 30% for testing (Hussain *et al.,* 2025; Huang *et al.,* 2020).

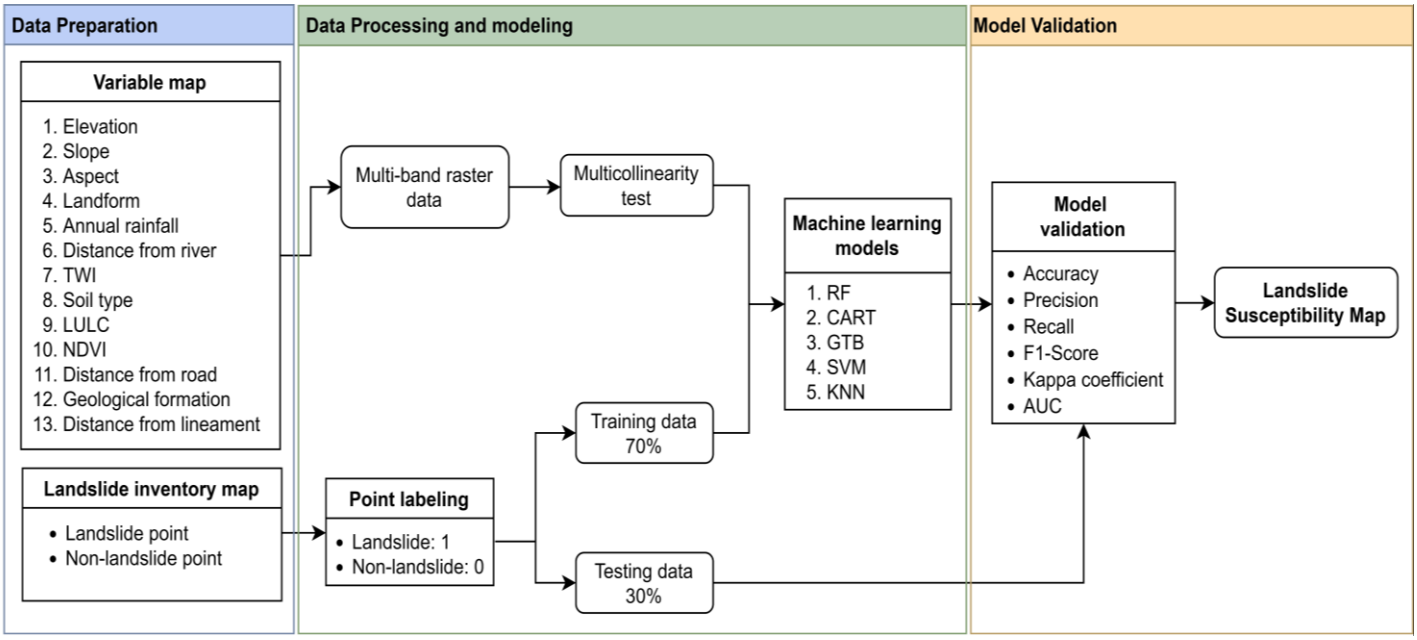

Figure 1. Landslide Susceptibility Mapping Flowchart.

This study evaluated five machine learning algorithms: RF, CART, GTB, SVM, and KNN. Model performance validation was conducted using several metrics: accuracy, precision, recall (sensitivity), F1-score, kappa coefficient, and area under the receiver operating characteristic (ROC) curve (AUC) (Hou *et al.,* 2025; Liang *et al.,* 2023). The results obtained were a landslide susceptibility map from each algorithm model, classified by area susceptibility level into five classes: very low, low, medium, high, and very high (Badapalli *et al.,* 2025; Suwarno *et al.,* 2025). This facilitated the identification of the area size of each landslide susceptibility class. A comparative analysis of these five maps could determine the most effective algorithm for the study area. The best of these will be used as a reference in analyzing variable importance so that the contribution of each factor to landslide susceptibility can be identified (Meena *et al.,* 2025; Qi *et al.,* 2024).

2.1. Study Area

The area of interest in this study was Batu City, East Java Province, Indonesia, located at 7°46′–7°55′S and 112°30′–112°39′E, with an area of ±199.09 km^2. There were 276 sample points in the area, consisting of 138 landslide (red dots) and 138 nonlandslide (green dots) points (Figure 2). This area was selected because of its high susceptibility to landslides. This susceptibility is mainly due to its physiographic conditions, as the area forms a topography with steep slopes due to the surrounding Mount Panderman, Mount Arjuno, and Mount Welirang. This topographic factor is also amplified by the elevation variation, which ranges from 680 to 1,200 m above sea level.

2.2. Conditioning Factors

This study utilized 13 conditioning factors, all of which were accessed and processed within the GEE cloud computing platform to ensure reproducibility and computational efficiency. All predictor variables used, along with their sources and spatial resolutions, are summarized in Table 1. Some data are available in raster format at varying resolutions (90–500 m), whereas other data are vector-based (e.g., distance from rivers, geological formations, and distance from lineaments). All vector data were converted to raster format, and all layers were resampled to a uniform spatial resolution (10 m) using the GEE platform to ensure that all variables share the same coverage and projection system. Once all conditioning factor maps were ready in the raster format, they were then combined into a single multiband image. This combination is necessary because machine learning algorithms require all input variables (predictors) for each pixel in the form of a single image with multiple channels (bands).

2.3. Data Preprocessing

Supervised machine learning models require labeled datasets for training. This study assigned two class labels to the samples: landslide points (1) and nonlandslide points (0). The distribution of landslide and nonlandslide sample points was sourced from the National Disaster Management Agency (BNPB) landslide potential inventory map, accessed through the InaRISK platform

(https://inarisk.bnpb.go.id). The dataset used consisted of 276 sample points, comprising 138 landslide points and 138 nonlandslide points. Both classes had the same number of points to produce an initial balance in the training data. To avoid class bias and ensure sample representativeness, stratified random sampling was applied to the dataset (Fu *et al.,* 2025; Zhou *et al.,* 2024). This approach ensured balanced representation of both classes. Finally, the entire dataset was divided into two parts at a 70:30 ratio, with 70% used as training data and 30% as testing data.

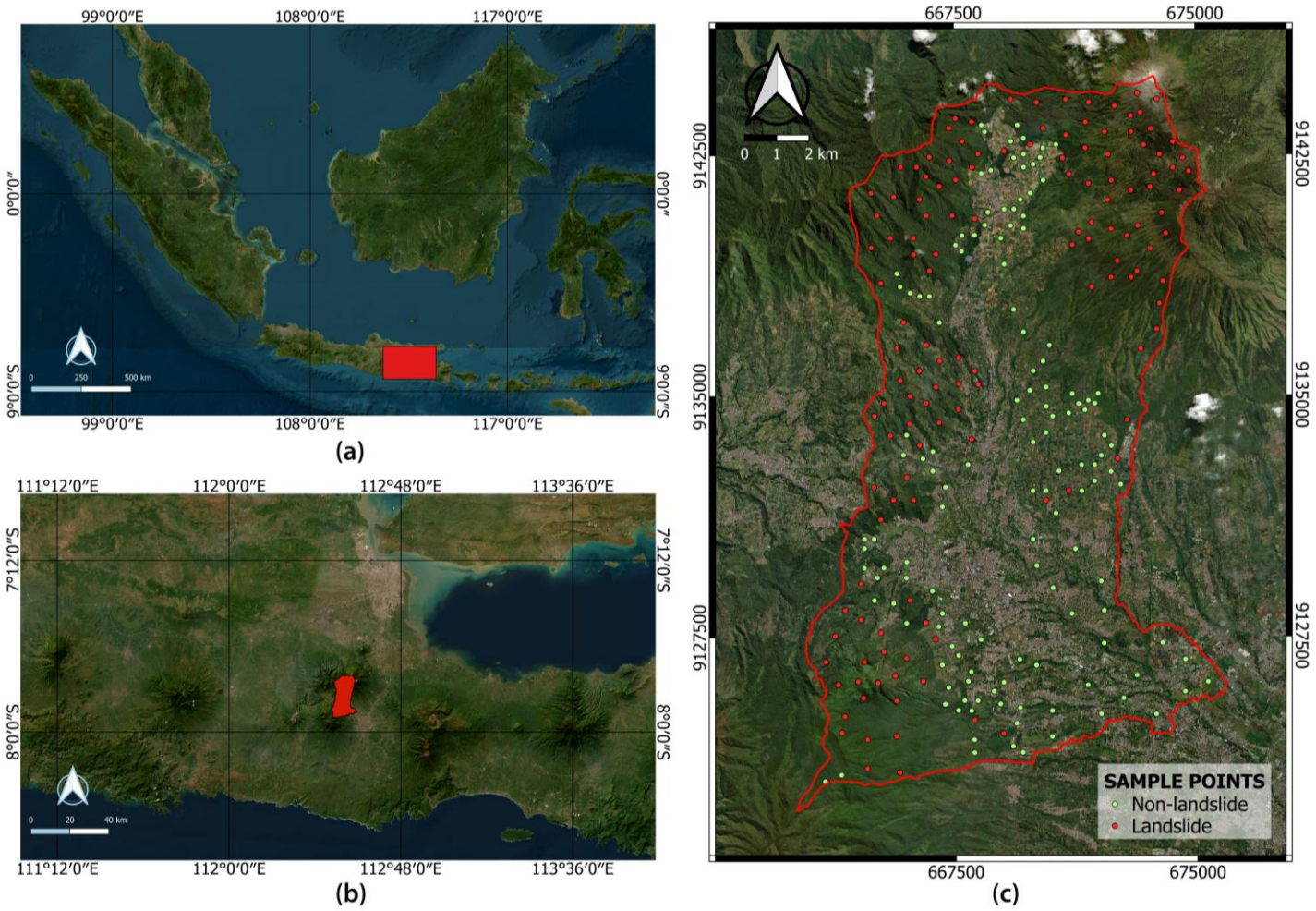

Figure 2. (a) Location of East Java Province. (b) Location of Batu City. (c) Study Area with 276 Sample Points, Consisting of 138 Landslides and 138 Nonlandslide Points.

Table 1. Conditioning Factors and Details Used in the Study.

Conditioning Factors	Source	Spatial resolution
Elevation	CGIAR SRTM V4	90 m
Slope	CGIAR SRTM V4	90 m
Aspect	CGIAR SRTM V4	90 m
Landform	CSP ALOS Lanforms	90 m
Annual rainfall	UCSB CHIRS Pentad	0.05°
Distance from rivers	WWF HydroSHEDS	Vector
TWI	WWF HydroSHEDS & CGIAR SRTM	15 arc-second
Soil type	FAO Harmonized World Soil Database v2	30 arc-second
LULC	MODIS Land Cover Type	500 m
NDVI	MODIS Vegetation Indices	250 m
Distance from roads	OpenStreetMap	Vector
Geological formation	Geological Research and Development Centre (PPPG)	Vector
Distance from lineaments	National Digital Elevation Model (DEMNAS)	Vector

2.4. Evaluation of Correlation Between Predictor Variables

Landslide susceptibility mapping in this study used 13 conditioning factors as predictor variables. In machine learning, they must be mutually independent and not strongly correlated (Qi *et al.,* 2021). Therefore, a Pearson correlation matrix of landslide predictor variables was used before

model formulation. Multicollinearity occurs when two variables in a multiple regression model are strongly correlated (Liu *et al.,* 2022). This process is essential in modeling to ensure the stability and reliability of the predictive model being formulated. The correlation matrix was calculated using all predictor variables. Correlation coefficient values above 0.7 indicated high multicollinearity (Ullah *et al.,* 2024).

2.5. Machine Learning Algorithms

The machine learning algorithms used in this study consisted of five models: RF, CART, GTB, SVM, and KNN. RF builds several decision trees on a random subset of the data and features and combines the voting results from these trees to produce a final decision (Le *et al.,* 2024; Khan *et al.,* 2021). Meanwhile, CART splits data using the Gini index, forming an easy-to-understand tree structure. The resulting tree model consists of internal nodes representing separation criteria and leaf nodes that contain class predictions (Zhou *et al.,* 2024). GTB operates through an iterative process; it builds a series of decision trees sequentially, with each new tree correcting the errors of the previous one (Tao *et al.,* 2022). All trees are combined using weighted ensemble prediction to gradually improve accuracy (Kavzoglu & Teke, 2022; Li *et al.,* 2025). SVM identifies the optimal hyperplane that maximizes the margin between the landslide and nonlandslide classes using support vectors (James *et al.,* 2013; Meena *et al.,* 2025). Finally, KNN predicts the value of a new observation based on the class or average of the nearest neighbors in feature space, usually calculated using Euclidean distance (Le *et al.,* 2024).

The optimal configurations for all machine learning models resulting from hyperparameter optimization are shown in Table 2. The RF model was configured with 100 decision trees and a seed value of 0. It produced an out-of-bag error of 0.114, indicating a good level of internal accuracy. The CART model adopted an ensemble approach comprising 193 trees, with a maximum structural restriction of 15 nodes and a maximum depth of 8 to control model complexity. This configuration balanced model complexity and prediction accuracy. The GTB model achieved optimal performance with 200 trees, a learning rate (shrinkage) of 0.05, and a sampling rate of 0.7. This configuration helped improve model stability. The SVM model used a linear kernel with a gamma of 0.005 and a cost (regularization parameter) of 1. It created an optimal decision boundary for class separation. Finally, the KNN model achieved the best performance with the number of neighbors (k) set to 10 and using the Manhattan metric. It was proven effective at handling high-dimensional data with 193 features. These optimized configurations ensured that each model could optimally extract patterns from the landslide distribution dataset.

Table 2. Hyperparameter Configurations for the Validated Classification Models.

Model	Parameters	Optimum
RF	Number of trees	100
	Seed	0
	Out-of-bag error	0.114
CART	Number of trees	193
	Max nodes	15
	Max depth	8
GTB	Number of trees	200
	Shrinkage (learning rate)	0.05
	Sampling rate	0.7
SVM	Kernel type	Linear
	Gamma	0.005
	Cost	1
KNN	*k*	10
	Metric	Manhattan
	Count features	193

2.6. Model Performance Validation

The evaluation matrix used to evaluate model performance includes accuracy, precision, recall (sensitivity), F1-score, kappa coefficient, and AUC. Figure 3 comprehensively compares the model predictions and actual values. The main components are true positive (TP), true negative (TN), false positive (FP), and false negative (FN). TP represents the correctly predicted positive cases (landslide points), whereas TN represents correctly predicted negative cases (nonlandslide points). Meanwhile, FP represents negative cases (nonlandslide points) that are predicted as positive (landslide points), whereas FN represents positive cases (landslide points) predicted as negative (nonlandslide points).

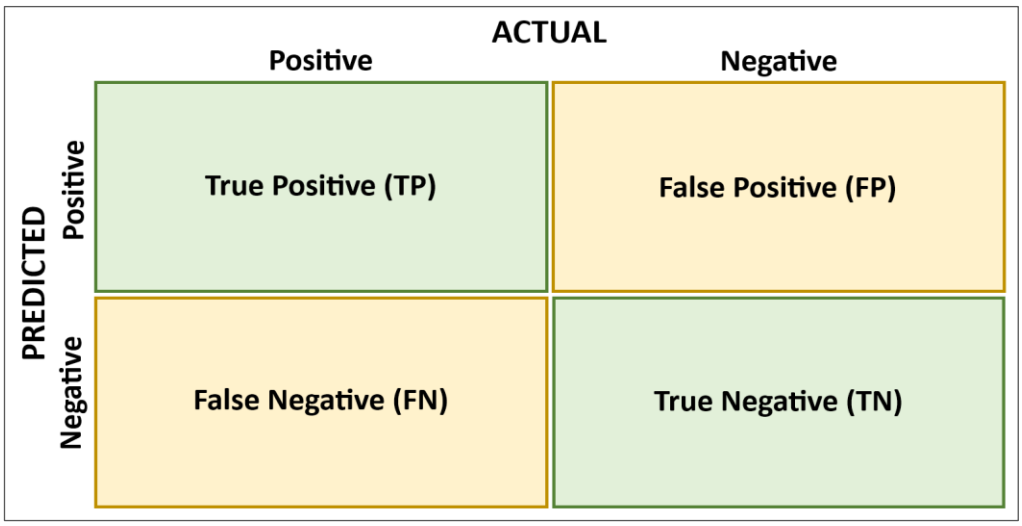

Figure 3. Table of Confusion Matrix.

The performances of the models were validated using various evaluation metrics: accuracy, precision, recall (sensitivity), and F1-score, as formulated in Equations (1)–(4) (Khadka *et al.,* 2025; Qiu *et al.,* 2024).

$$Accuracy = \frac{TP + TN}{TP + TN + FP + FN} \quad (1)$$

$$Precision = \frac{TP}{TP + FP} \quad (2)$$

$$Recall = \frac{TP}{TP + FN} \quad (3)$$

$$F1\text{-}score = \frac{2 * Precision * Recall}{Precision + Recall} \quad (4)$$

In addition, the performances of the models obtained were validated using the kappa coefficient, as shown in Equation (5) (Khadka *et al.,* 2025). This metric can provide a more reliable description of the model's predictive performance, especially for unbalanced data. In some cases, it is considered the standard metric for model comparison.

$$Kappa = \frac{Total\ Agreement - Agreement\ by\ chance}{1 - Agreement\ by\ chance} \quad (5)$$

Where

$$Total\ Agreement = \frac{TP + TN}{TP + TN + FN + FP} \quad (6)$$

And

$$Agreement\ by\ chance = \frac{[(TP + FP) \times (TP + FN) \times (FN + TN) \times (FP + TN)]}{(TP + FP + TN + FN)^2} \quad (7)$$

This metric is considered more reliable than accuracy because it accounts for agreement occurring by chance. Model performance is generally described on a scale from 0 to 1, as shown in Table 3 (Landis & Koch, 1977).

Finally, model performance was also validated using ROC curves. The model with the highest AUC value and optimum balance between precision and recall was considered the most representative model. Spatial validation was applied using spatial cross-validation techniques to reduce the effects of spatial autocorrelation (spatial overfitting) and improve prediction reliability (Le *et al.,* 2024; Tjahjono *et al.,* 2024).

Table 3. Model Performance Based on the Kappa Coefficient Scale (Landis & Koch, 1977).

No.	Value range	Level of agreement
1	0.00–0.20	Slight agreement
2	0.21–0.40	Fair agreement
3	0.41–0.60	Moderate agreement
4	0.61–0.80	Substantial agreement
5	0.81–1.00	Almost perfect agreement

3. Results and Discussion

3.1. Map of Landslide Predictor Variables

Spatially, the maps of the 13 predictor variables were generated in QGIS 3.34 using the UTM 49S projection, which was appropriate for the study area. The type of spatial data and the grid resolution produced varied according to the data available on the GEE platform. They showed consistent geographic coverage, confirming the spatial alignment among predictor layers—a key precondition for reliable pixel-based modeling. Each map represented a predictor, with the distribution of values visualized through color gradients. This visual inventory facilitated a qualitative assessment of spatial heterogeneity across the study area. In addition, it enabled the identification of potential multicollinearity among predictor variables before performing quantitative hyperparameter optimization. The 13 predictor maps produced in the study are shown in Figure 4.

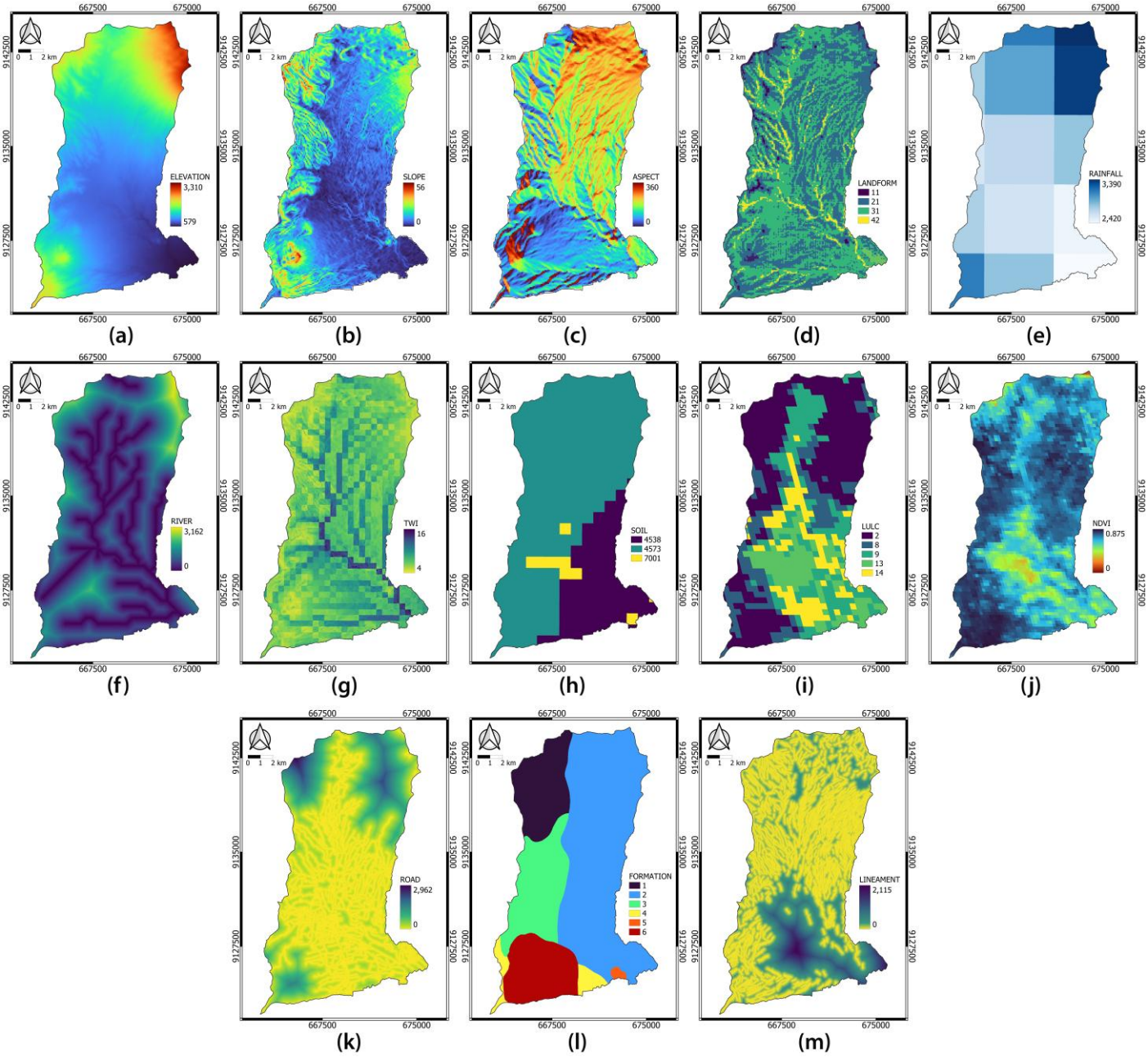

Figure 4. Predictor Variables of Landslide in This Study: (a) Elevation, (b) Slope, (c) Aspect, (d) Landforms, (e) Annual Rainfall, (f) Distance from Rivers, (g) TWI, (h) Soil Types, (i) LULC, (j) NDVI, (k) Distance from Roads, (l) Geological Formations, and (m) Distance from Lineaments.

3.2. Correlations Between the Landslide Predictor Variables

The significance of the correlations between the landslide predictor variables, as quantified using the Pearson correlation matrix, is presented in Figure 5. The elevation variable exhibited a strong

positive correlation with annual rainfall ($r = 0.88$). Meanwhile, the strong correlation between elevation and annual rainfall exceeded the specified threshold (Ullah *et al.*, 2024; Qi *et al.*, 2021). Therefore, to avoid multicollinearity problems due to strong correlation, one of them was eliminated. This study retained the elevation variable and eliminated the rainfall variable from the model. The elevation variable also showed a strong positive correlation with distance from rivers ($r = 0.64$) and distance from roads ($r = 0.60$). These suggest that areas with high elevation tend to experience greater precipitation intensity and are often spatially proximal to drainage systems and road infrastructure.

In contrast, geological formation with distance from rivers ($r = -0.00$) and slope ($r = 0.03$) showed very weak correlations. In addition, soil type and landforms exhibited a very weak correlation with most other predictors, as reflected in the correlation values of soil type with landforms ($r = 0.01$) and geological formation ($r = -0.01$), and landforms with distance from roads ($r = 0.01$). A similar pattern was also observed for NDVI and aspect, which showed no significant relationship with many other variables. Furthermore, significant inverse relationships were observed. The negative correlation between LULC and distance from roads ($r = -0.59$) suggests that certain land cover types tend to occur farther from roads. Similarly, the negative correlation between TWI and slope ($r = -0.58$) indicates that steeper slopes consistently correspond to lower TWI values. By eliminating the annual rainfall variable, the correlations obtained between the predictor variables were less than the threshold of 0.7, confirming the multivariable interdependence in the slope system. This was done to emphasize the importance of selecting predictor variables to avoid multicollinearity in landslide susceptibility mapping.

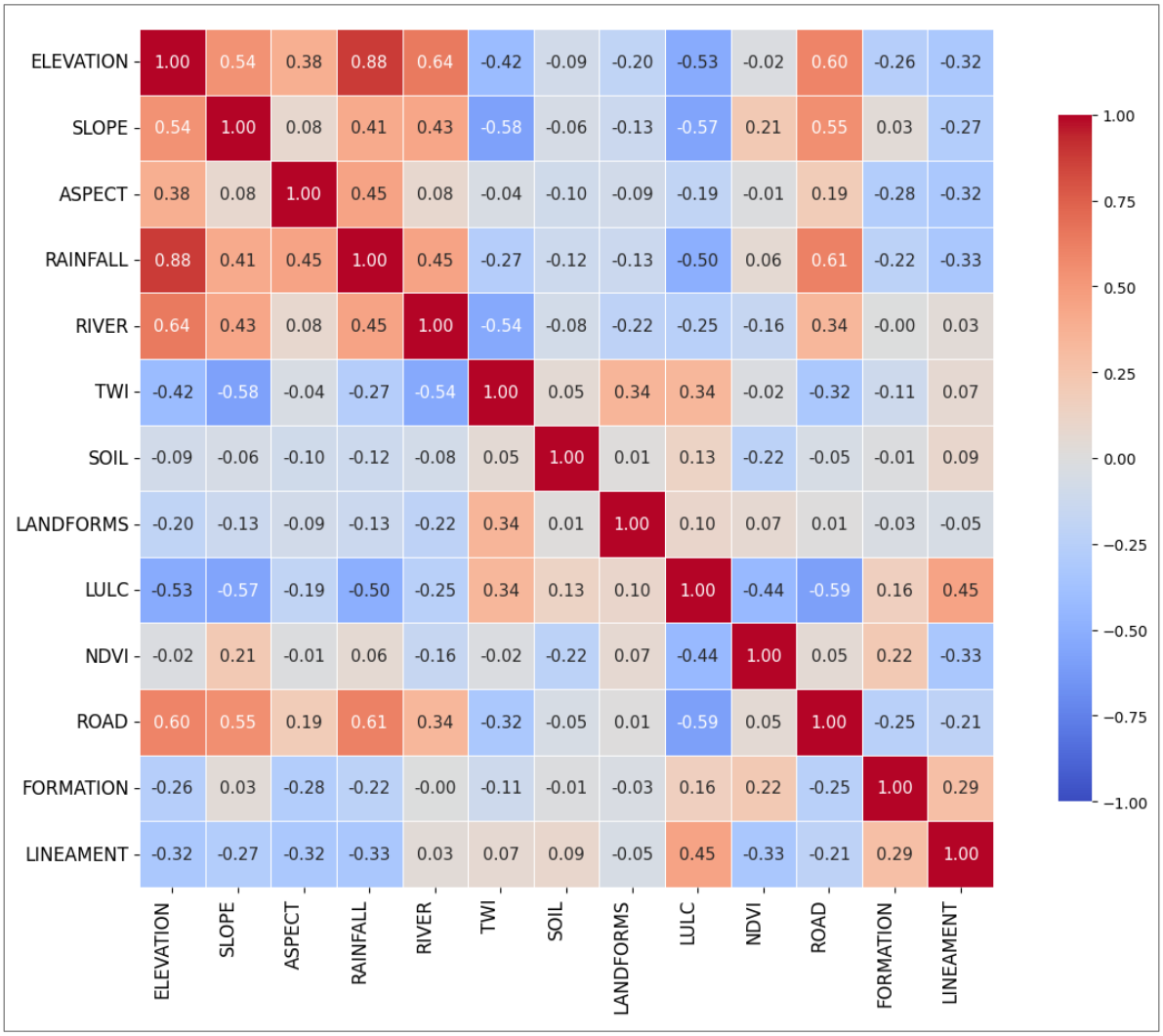

Figure 5. Pearson Correlation Matrix of the Landslide Predictor Variables.

3.3. Landslide Susceptibility Map

Landslide susceptibility mapping was conducted using the results of a Pearson correlation matrix analysis, where annual rainfall data were excluded to avoid multicollinearity. This resulted in 12 predictors used for mapping: elevation, slope, aspect, landforms, distance from rivers, TWI, soil

types, LULC, NDVI, distance from roads, geological formations, and distance from lineaments. The maps generated by each algorithm are illustrated in Figure 6, showing varying distributions of susceptibility classes. The maps produced by RF and GTB exhibit a more concentrated distribution of areas with high and very high susceptibility. This indicates better consistency in susceptibility zone identification compared with the other models. In contrast, the maps produced by CART and KNN tend to display more scattered and fragmented patterns, with high susceptibility spread across several locations. In addition, SVM shows a relatively moderate distribution pattern compared with the other models. These pattern differences indicate variations in the algorithms' ability to process nonlinear relationships between variables. The spatial distribution patterns on the landslide susceptibility maps indicate that areas with high and very high susceptibility classes in Batu City are concentrated in zones with steep slopes. These high-risk areas dominate the complex topography formed by the presence of young Quaternary volcanoes—namely, Mount Panderman, Mount Arjuno, and Mount Welirang.

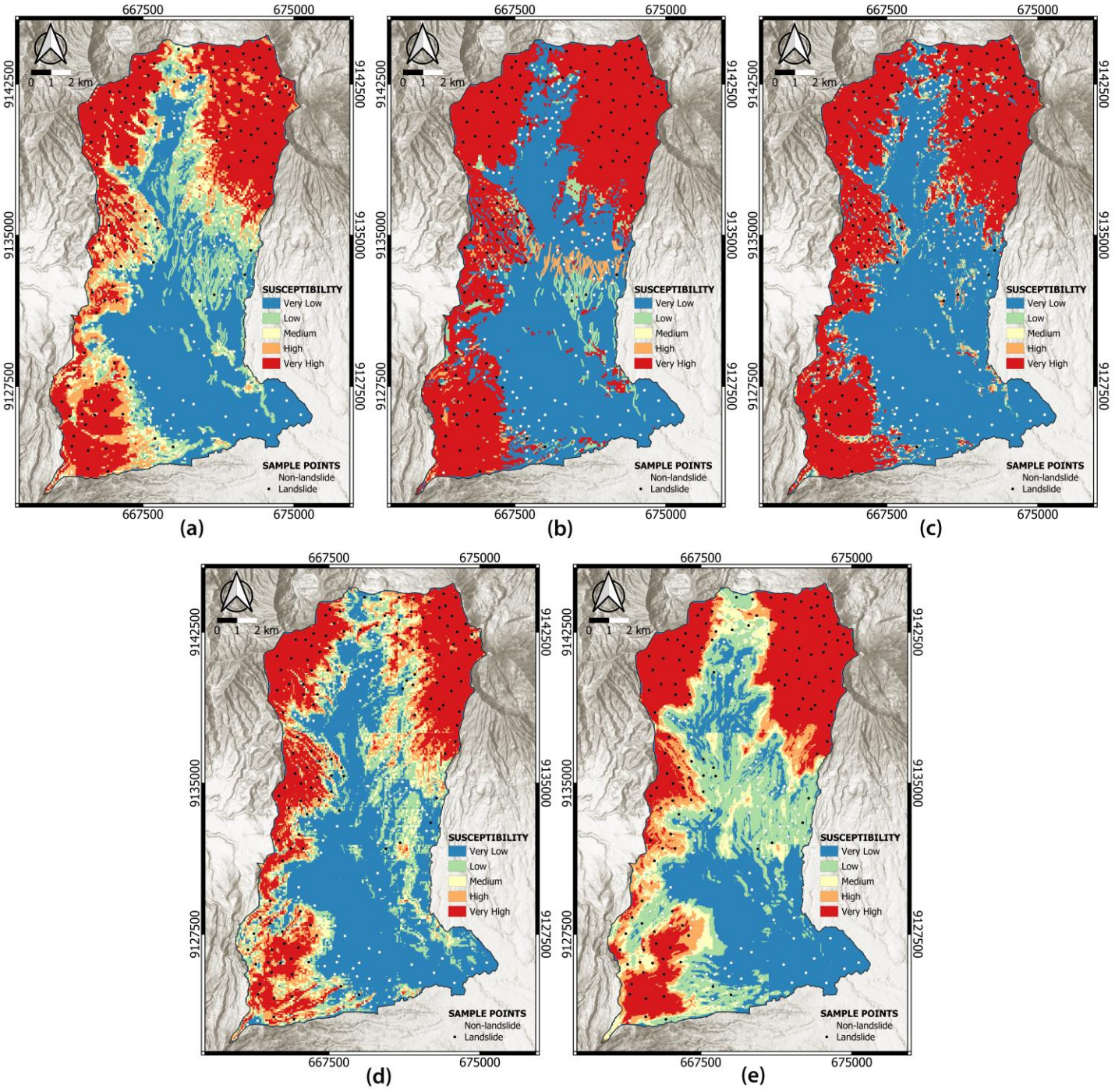

Figure 6. Landslide Susceptibility Maps of the Studied Algorithms: (a) RF, (b) CART, (c) GTB, (d) SVM, and (e) KNN.

The percentage areas of the susceptibility classes generated by the five models are presented in Figure 7. Based on the total area of Batu City (199.09 km^2), the RF model showed the most balanced distribution, with significant portions in the very high class (60.70 km^2 or 30.49%) and very low class (70.16 km^2 or 35.24%), indicating its good ability to differentiate between each class. In contrast, CART and GTB showed strong polarization trends, with a dominance of the very high class of 89.94 km^2 (45.18%) and 83.74 km^2 (42.06%), respectively, and a lack of representation of the medium class, indicating their tendency to overpredict the very low or very high classes. SVM produced a relatively even distribution across all susceptibility classes, with peaks in the very low (80.38 km^2 or 40.37%) and very high (49.56 km^2 or 24.89%) classes, reflecting moderate characteristics in susceptibility classification. Furthermore, KNN showed the highest concentration in the very low (59.61 km^2 or 29.94%) and low (45.99 km^2 or 23.10%) classes, indicating that it was more conservative than the other models in predicting high-risk zones. These results show significant variations in classification across models. According to the distribution of landslide susceptibility classes, the RF model presents the best and most realistic distribution. Therefore, the selection of this model must consider the distribution of areas within each class to align with the decision-making context for risk-based mitigation.

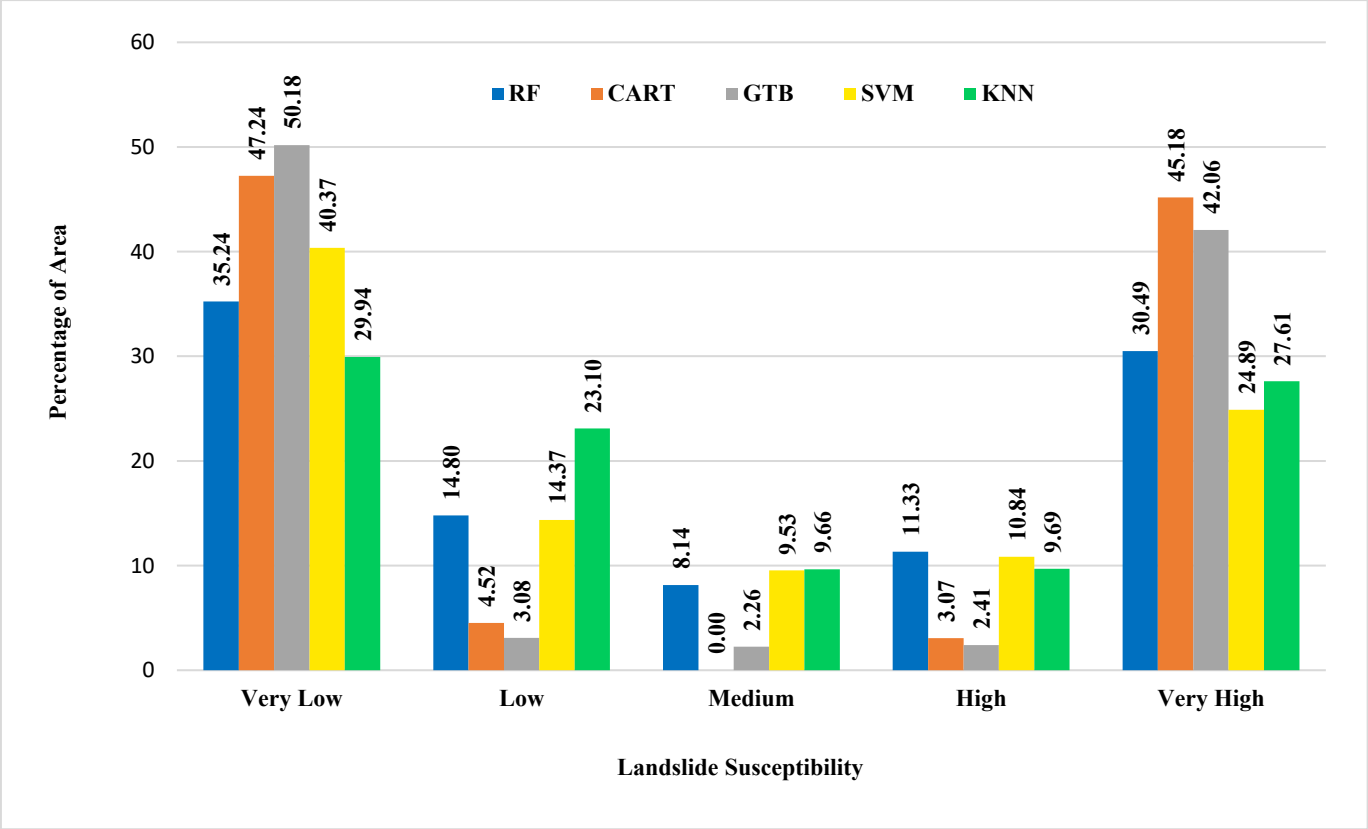

Figure 7. Percentages of Landslide Susceptibility Areas Generated by the Models.

3.4. Results of Model Performance Validation

The results for 83 testing datasets using the five algorithm models are shown in a confusion matrix (Table 4). These results indicate that RF achieved the best performance, with TP and TN of 35 and 43, respectively. This model also had the lowest total classification errors (FP and FN) of 5, followed by GTB with a total error of 7. In addition, CART and SVM tended to have higher FN—8 and 9 points, respectively. These indicate the model's inability to detect positive instances. KNN had a high TN (43 points) but the highest FP (10 points). These indicate the error rate in predicting negative instances. Thus, RF and GTB are more reliable and balanced approaches for the tested datasets.

Table 4. Confusion Matrix Produced by Testing Data

Model	TP	FP	FN	TN
RF	35	2	3	43
CART	33	4	8	38
GTB	34	3	4	42
SVM	32	5	9	37
KNN	27	10	3	43

Based on the comprehensive analysis using 83 testing data points (representing 30% of the total data), RF demonstrated the best performance compared with the other four models. This model produced the highest values for accuracy (0.940), precision (0.946), recall (0.921), F1-score (0.933), and kappa coefficient (0.878), as shown in Table 5. Therefore, it is the most reliable and robust at identifying patterns in the testing data among all studied models (Melati *et al.,* 2024). Its high accuracy and precision indicate that it can make accurate predictions overall and minimize false-positive classification errors. In addition, it produces high recall, indicating its ability to detect almost all truly positive instances (minimizing FNs). Moreover, the high kappa coefficient confirms that the level of agreement between the model's predictions and the actual conditions falls into the almost perfect agreement category, exceeding what would be expected by chance (Landis & Koch, 1977).

The second-best model after RF was GTB. It performed strongly and was a balanced and effective predictor. In contrast, KNN, despite having a high recall of 0.900, had a relatively low precision of 0.730. This high FP rate makes its positive predictions less reliable. These results indicate its weakness: it tends to be overly aggressive in assigning positive labels, resulting in many FPs. Meanwhile, CART and SVM showed moderate capabilities but were less consistent than the other models. Therefore, apart from RF, the advantage of GTB over CART, SVM, and KNN lies in its ability to maintain the right balance between accuracy and reliability.

Table 5. Model Performance Validation.

Model	Accuracy	Precision	Recall (sensitivity)	F1-score	Kappa coefficient
RF	0.940	0.946	0.921	0.933	0.878
CART	0.855	0.892	0.805	0.846	0.711
GTB	0.916	0.919	0.895	0.907	0.830
SVM	0.831	0.865	0.781	0.821	0.662
KNN	0.843	0.730	0.900	0.806	0.677

The ROC curves for landslide susceptibility prediction for the five models are shown in Figure 8. The results show that RF achieved the highest AUC of 0.976. It is regarded as the best classifier for mapping landslide susceptibility, particularly in the study area. The AUC value quantifies the probability that a model can randomly rank positive instances with higher scores than negative instances. Thus, a value of 0.976 indicates an excellent separation ability of 97.6%. The level of discrimination ensures that the resulting landslide susceptibility map can effectively differentiate between high- and low-susceptibility zones, providing a credible basis for field mitigation planning. The discriminatory performance of RF also exceeded that of the other models, such as GTB (0.962), CART (0.930), SVM (0.927), and KNN (0.900). This excellent AUC performance reinforces the conclusions drawn from the previous evaluation metrics, providing comprehensive confirmation that RF is the most optimized and consistent model in the overall performance assessment. Thus, the landslide susceptibility map and variable importance results of RF are selected for subsequent analyses.

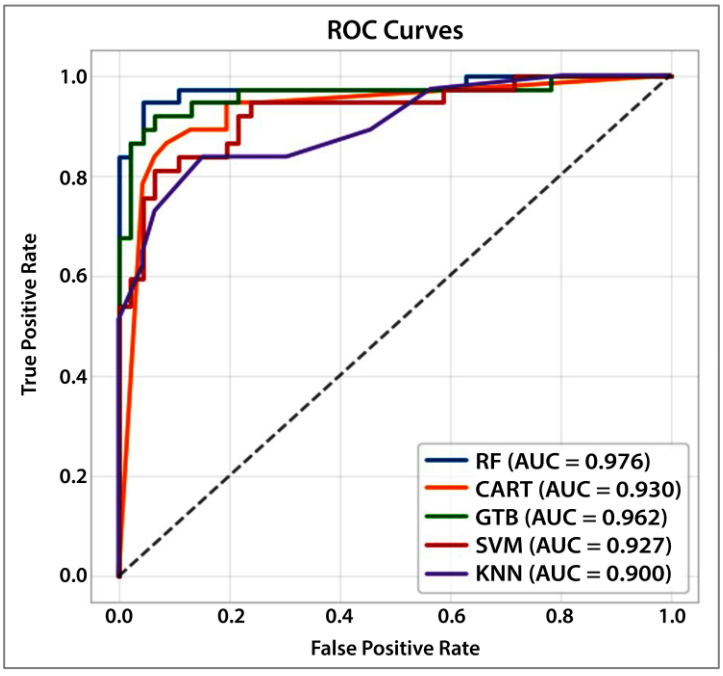

Figure 8. ROC Curves of the Landslide Prediction Models.

3.5. Variable Importance

The results of the variable importance analysis of RF in landslide susceptibility mapping are shown in Figure 9. Based on the variable importance, the total accumulated mean decrease in impurity value for all variables was 285.02. The slope variable exhibited the most significant contribution, with a mean decrease in impurity value of 43.77, equivalent to 15.36% of the total importance. This result indicates that slope is the main controlling factor of landslides, as it can affect slope stability. This is because it can affect shear stress and soil mass stability (Zeng *et al.,* 2024). The mean decrease in impurity measures the total reduction in impurity achieved by each variable across the entire ensemble tree. A higher value generally indicates stronger predictive power (Breiman *et al.,* 1984).

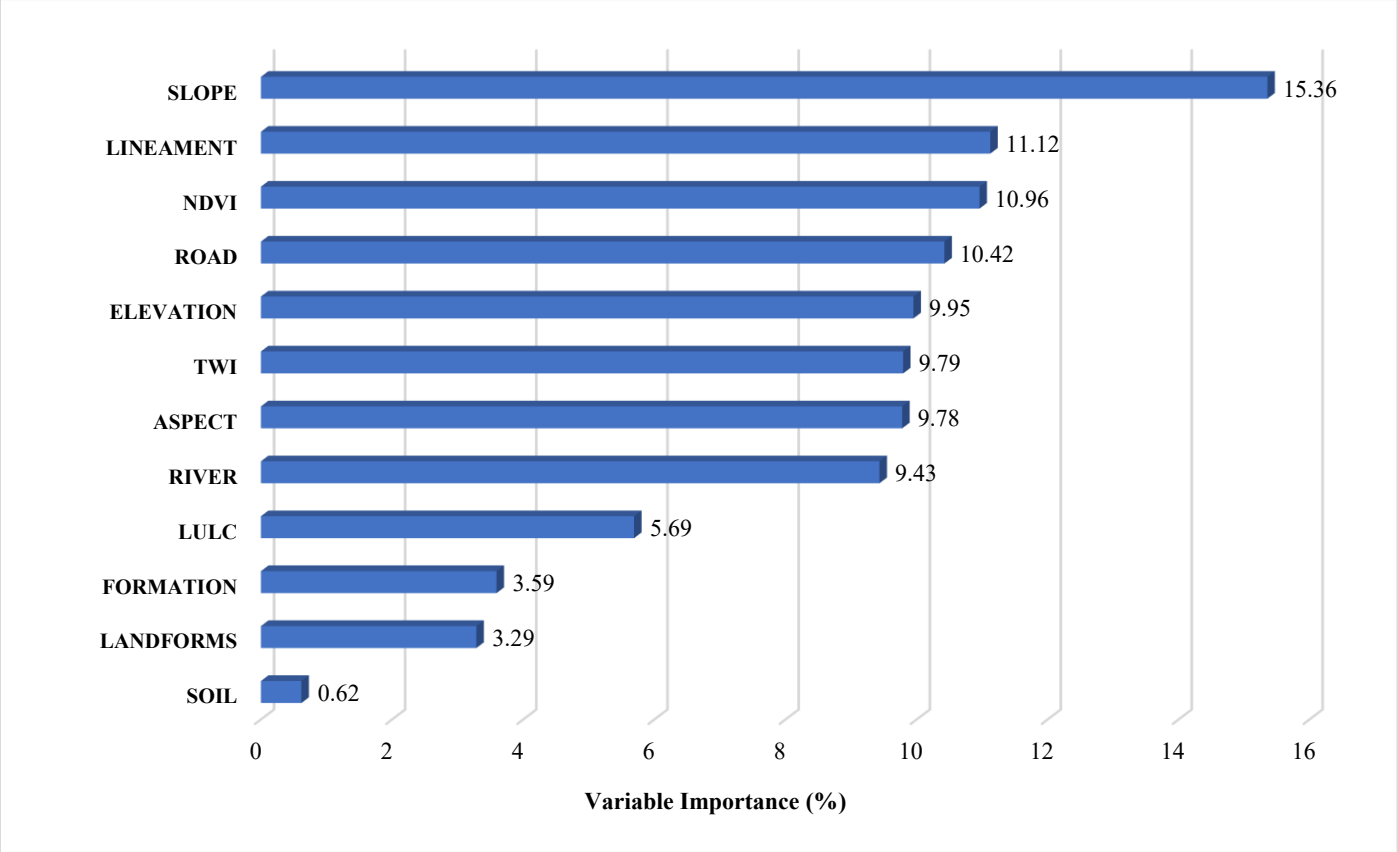

Figure 9. Variable Importance of the RF Model.

In addition, the other variables that contributed to landslide susceptibility after the slope variable were distance from lineaments (11.12%), NDVI (10.96%), distance from roads (10.42%), elevation (9.95%), TWI (9.79%), aspect (9.78%), and distance from rivers (9.43%). They showed the complexity of factors influencing landslide susceptibility in the study area. The influence of the lineament variable, which ranked second-highest, indicated the role of geological structures in underground water flow control and the formation of weak zones in rocks. In contrast, the NDVI variable reflected vegetation's role in stabilizing slopes through root systems and rainfall interception (Pappaka *et al.,* 2025; Hussain *et al.,* 2022). The influence of the distance from roads variable indicated that human activity, infrastructure, and vehicles can destabilize slopes by increasing loads in landslide-prone areas (Ersayin & Uzun, 2025; Qi *et al.,* 2024). TWI and distance from rivers both indicated the influence of hydrological conditions on pore water pressure, which is the main trigger of soil mass movement (Nurwatik et al., 2022; Xu *et al.,* 2022).

Finally, the remaining variables exhibited lower importance values, including LULC (5.69%), geological formation (3.59%), landforms (3.29%), and soil type (0.62%). These results also indicate that morphometric variables, including slope, TWI, aspect, and proximity features (distance from lineaments, roads, and rivers), have stronger predictive capabilities than inherent material characteristics (geological formation and soil type) and landform classification. This is probably due to the homogeneity of geological and soil characteristics in the study area and the low data resolution, which is insufficient to capture variations in material properties at this mapping scale. Furthermore, variables such as geological formation and soil type may be more static and less spatial than morphometric parameters that directly reflect slope stability conditions.

These results indicate that the landslide susceptibility modeling approach in the study area is more effective when it focuses on topographic characteristics and proximity factors that are more responsive to spatial changes in slope conditions.

3.6. Discussion

Based on model performance evaluation metrics, RF achieved the best overall performance for landslide susceptibility in Batu City. The advantage of RF's ensemble nature is that it can build multiple decision trees from randomized subsets of data and features, thereby reducing the risk of overfitting and improving prediction stability (Liu *et al.,* 2022). Furthermore, its ability to handle complex (nonlinear) relationships between landslide variables and its strong discriminatory power result in a balanced and proportional distribution of each susceptibility class. This aligns with previous studies confirming that RF outperforms other algorithms for landslide susceptibility mapping in tropical volcanic regions, as evidenced by its high AUC (Melati *et al.,* 2024; Wu *et al.,* 2022). However, some previous studies reported that GTB was slightly superior to RF (Kavzoglu & Teke, 2022). This contradiction is likely due to differences in the study area's characteristics, which featured steeper slopes and more heterogeneous land use. The RF bagging mechanism provides better stability against extreme gradient values, whereas the boosting approach in the GTB tends to amplify errors from outliers (Liu *et al.,* 2022). Thus, tree-based ensemble algorithms, particularly RF, achieve excellent results with hyperparameter optimization, further strengthening the justification for the model selection in this study.

The variable importance analysis identified the most influential variables for landslide potential. In particular, the slope angle directly affects shear stress and soil stability (Zeng *et al.,* 2024). Consequently, steep slopes amplify gravitational forces, which can trigger soil movement. The volcanic material in this area is highly weathered and poorly consolidated, making the slope composition vulnerable. If these conditions are present on a steep slope, the shear stress will naturally approach or exceed the soil's shear strength (Muhardi & Perdhana, 2025). This situation becomes even riskier when triggered by external factors, such as rain or anthropogenic activities (Hasan *et al.,* 2024). This explains why the slope variable had the highest importance compared with the other variables (Ersayin & Uzun, 2025). Therefore, mitigation efforts can be implemented by focusing on slope stabilization and land use in topographic zones with extreme slopes.

Although slope is often identified as a dominant factor in various landslide susceptibility studies, the dominance of a factor is highly determined by local geological, climatic, and anthropogenic characteristics (Pasang & Kubíček, 2020; Arabameri *et al.,* 2020). In areas with homogeneous volcanic material, structural parameters (e.g., distance to lineaments and NDVI) are more influential than soil type or geological formation. In contrast, in areas with high human activity, distance from roads and land cover become the primary factors, even surpassing slope (Pasang & Kubíček, 2020). In tectonically active regions, distance from roads and NDVI dominate, whereas elevation and distance from rivers play a greater role in reservoir areas because of periodic water level fluctuations (Qi *et al.,* 2024; Zhou *et al.,* 2024). Furthermore, optimizing environmental factors reportedly improves modeling accuracy—that is, elevation and lithology can exhibit influence comparable to that of slope (Li *et al.,* 2025). Thus, although slope is a dominant factor, it is not absolute and depends on environmental conditions, triggering mechanisms, and the quality of the data used.

The landslide susceptibility distribution pattern in the study area shows that high and very high classes are generally found on steep mountain slopes. This is consistent with the variable importance analysis, which identified slope as the dominant factor. This is because areas with high susceptibility are generally formed by the presence of a series of young Quaternary volcanoes, such as Mount Panderman, Mount Arjuno, and Mount Welirang. They can produce volcanic materials, such as ash, lapilli, breccia, and tuff, which are not yet properly consolidated (Noviyanto *et al.,* 2020). These young volcanic materials have high porosity, facilitating rainwater absorption, which then increases pore water pressure and soil mass weight. These conditions produce loose, easily eroded materials susceptible to weathering, reducing slope stability in steep areas (Susilo *et al.,* 2023). The combination of loose material properties and steep slope accelerates destabilization in the study area.

Classification on the GEE platform is inherently limited to pixel-level predictions and is unable to capture more detailed spatial information (e.g., slope connectivity or landslide paths). Consequently, pixel-based models, including those used in this study, tend to overlook the connectivity between upper and lower slopes. This limitation significantly affects the results, as failures in the upper slope often affect lower-slope areas (Wu *et al.,* 2022). To address this, future studies should use slope units as the mapping unit instead of grid cells and include spatial

validation. From a practical perspective, the susceptibility map generated in this study identifies an area of 70.16 km^2 (35.24%) as a very-high-susceptibility zone. These results can serve as a basis for disaster mitigation strategies, including slope stabilization, land-use zoning, and the development of early warning systems, in line with recommendations to integrate landslide susceptibility mapping into regional spatial planning (Tjahjono *et al.,* 2024). However, the application of this model to other volcanic regions remains dependent on recalibrating the relevance of predictors and the quality of local data, as machine learning performance is highly sensitive to spatial resolution and the completeness of the data inventory (Hussain *et al.,* 2025; Zhou *et al.,* 2024). Furthermore, the landslide inventory in this study still relied on historical point data from the BNPB's InaRISK platform. Therefore, direct field surveys are essential to ensure that landslide sample points are in areas that have experienced landslide events and to confirm and assess the potential for future landslides.

To improve data accuracy in landslide area inventories, future studies should integrate high-resolution datasets (e.g., drone-based digital elevation model mapping, direct field soil sampling, and laboratory soil testing) with dynamic factors, including multitemporal rainfall, land cover changes, and InSAR techniques. Additionally, this study identified slope, lineament density, and NDVI as dominant factors influencing landslides, enabling the implementation of phased, spatially tailored interventions. For example, areas with high lineament density require detailed field geological mapping to identify weak zones, whereas areas with low NDVI should be a priority for large-scale reforestation. Furthermore, susceptibility maps can be integrated into rainfall-based landslide early warning systems by setting rainfall thresholds in the study area based on landslide history. Finally, as a disaster mitigation strategy, these results can guide infrastructure zoning by avoiding the construction of new roads or the expansion of residential settlements in high-risk areas, thereby reducing future risks.

4. Conclusion

In this study, landslide susceptibility mapping was produced using machine learning on the GEE platform. It applied and compared five algorithms: RF, CART, SVM, GTB, and KNN. This study used 276 datasets, consisting of 138 landslide and 138 nonlandslide points, split 70% for training and 30% for testing. Landslide susceptibility maps were generated using 12 conditioning factors: elevation, slope, aspect, distance from rivers, TWI, soil type, landform, LULC, NDVI, distance from roads, geological formations, and distance from lineaments. The best model was determined using several evaluation metrics, including accuracy, precision, recall (sensitivity), F1-score, kappa coefficient, and AUC. The model evaluation metrics indicated that RF outperformed all other algorithms. The distribution of landslide susceptibility based on RF showed an area with a very low landslide susceptibility class of 60.70 km^2 (30.49%), a low class of 29.47 km^2 (14.80%), a medium class of 16.21 km^2 (8.14%), a high class of 22.56 km^2 (11.33%), and a very high class of 70.16 km^2 (35.24%). Variable importance analysis revealed that slope was the most influential variable, with a mean decrease in impurity value of 43.77 (15.36%). Meanwhile, soil type had the lowest contribution, with a mean decrease in impurity value of 1.77 (0.62%). The cloud-based machine learning framework developed in this study is transferable and can be adapted to other landslide-prone areas, particularly in tropical volcanic regions. This approach provides a reproducible and low-cost solution for disaster risk reduction and evidence-based land-use planning in regions facing similar hydrometeorological hazards.

Acknowledgements

The authors gratefully acknowledge the scholarship and study funding support from the Indonesian Education Scholarship (BPI), the Center for Higher Education Funding and Assessment (PPAPT) of the Ministry of Higher Education, Science, and Technology, and the Endowment Fund for Education Agency (LPDP) of the Ministry of Finance, Republic of Indonesia.

Author Contributions

Conceptualization: Susilo, A.; Suryo, E. A., Putra Y. S. **methodology**: Muhardi, Sutasoma, M., Bery, A. A., Hasan, M. F. R.; **investigation**: Muhardi, Nugraha, R. P.; **writing—original draft preparation**: Muhardi; **writing—review and editing**: Muhardi, Faizal, R.; **visualization**: Muhardi, Lestari, N. A. G.

All authors have read and agreed to the published version of the manuscript.

Conflict of interest

All authors declare that they have no conflicts of interest.

Funding

This study was funded by the Indonesian Education Scholarship (BPI) of the Ministry of Higher Education, Science, and Technology, Republic of Indonesia.

References

Agung, P. A. M., Hasan, M. F. R., Susilo, A., Ahmad, M. A., Ahmad, M. J. B., Abdurrahman, U. A., Sudjianto, A. T., & Suryo, E. A. (2023). Compilation of Parameter Control for Mapping the Potential Landslide Areas. *Civil Engineering Journal*, 9(4), 974–989. doi: 10.28991/CEJ-2023-09-04-016

Ali, N., Chen, J., Fu, X., Ali, R., Hussain, M. A., Daud, H., Hussain, J., & Altalbe, A. (2024). Integrating Machine Learning Ensembles for Landslide Susceptibility Mapping in Northern Pakistan. *Remote Sensing*, 16(6), 1–27. doi: 10.3390/rs16060988

Anuragi, S. K. (2025). Geospatial and Optimized SVM-Based Landslide Susceptibility Zonation of South District of Sikkim, India. *Geomatics and Environmental Engineering*, *19*(3), 115–141. doi: 10.7494/geom.2025.19.3.115

Arabameri, A., Saha, S., Roy, J., Chen, W., Blaschke, T., & Bui, D. T. (2020). Landslide Susceptibility Evaluation and Management Using Different Machine Learning Methods in The Gallicash River Watershed, Iran Alireza. *Remote Sensing*, 12(3), 1–29. doi: 10.3390/rs12030475

Asmare, D., Tesfa, C., & Zewdie, M. M. (2023). GIS-Based Landslide Susceptibility Assessment and Mapping. *Applied Geomatics*, 15, 265–280. doi: 10.1007/s12518-023-00499-7

Ayala, I. A. (2025). Landslides in a Changing World. *Landslides*, *22*(9), 2851–2865. doi: 10.1007/s10346-024-02451-1

Badapalli, P. K., Nakkala, A. B., Kottala, R. B., Gugulothu, S., Hasher, F. F. Ben, Mishra, V. N., & Zhran, M. (2025). Landslide Susceptibility Level Mapping in Kozhikode, Kerala, Using Machine Learning-Based Random Forest, Remote Sensing, and GIS Techniques. *Land*, 14(7), 1–25. doi: 10.3390/land14071453

Bagaskoro, Y., Adi, A. W., Wibawant, P., Yulistya, V. D., Sari, A. N., Purnamasiwi, D. I., Hafizh, A., Siambaton, H. M., Putra, A. S., Jayanti, T., Dewi, A. N., Karimah, R., Eveline, F., Ayu, H., Rizqi, A., Alfian, A., Fatah, H., Selina,

D. C., Avinnata, H., … Seniarwan. (2025). *Indeks Risiko Bencana Indonesia Tahun 2024* (Vol. 3, Issue 3). Badan Nasional Penanggulangan Bencana.

Breiman, L., Friedman, J. H., Olshen, R. A., & Stone, C. J. (1984). *Classification and Regression Trees*. Chapman and Hall/CRC.

Chen, Y. (2025). Spatial Prediction and Mapping of Landslide Susceptibility Using Machine Learning Models. *Natural Hazards*, 121, 8367–8385. doi: 10.1007/s11069-025-07132-3

Ersayin, K., & Uzun, A. (2025). A Comprehensive Analysis of Landslide Susceptibility in Iyidere Basin (NE, Turkey) Using Machine Learning Techniques and Statistical Bivariate Methods. *Natural Hazards*, 121(12), 1–38. doi: 10.1007/s11069-025-07354-5

Fu, Y., Fan, Z., Li, X., Wang, P., Sun, X., Ren, Y., & Cao, W. (2025). The Influence of Non-Landslide Sample Selection Methods on Landslide Susceptibility Prediction. *Land*, 14(4), 1–21. doi: 10.3390/land14040722

Hasan, M. F. R., Susilo, A., Suryo, E. A., Agung, P. A. M., Wiyono, Pratiwie, D. L., & Dewi, N. M. (2024). Assessment and Simulation of Potential Landslide Caused by the Rainfall Intensity in Batu City During 2021. *IOP Conference Series: Earth and Environmental Science*, 1314(012017), 1–9. doi: 10.1088/1755-1315/1314/1/012017

Heo, S., Sohn, W., Park, S., & Kun, D. (2024). Multi-Hazard Assessment for Flood and Landslide Risk in Kalimantan and Sumatra: Implications for Nusantara, Indonesia's New Capital. *Heliyon*, *10*(18), 1–17. doi: 10.1016/j.heliyon.2024.e37789

Highland, L. M., & Bobrowsky, P. (2008). *The Landslide Handbook: A Guide to Understanding Landslides*. U.S. Geological Survey.

Hou, C., Liu, H., Wang, X., Hu, J., Tang, Y., & Yao, X. (2025). Landslide Susceptibility Analysis Based on Dataset Construction of Landslides in Yiyang Using GIS and Machine Learning. *Applied Sciences*, 15(10), 1–29. doi: 10.3390/app15105597

Huang, F., Cao, Z., Guo, J., Jiang, S. H., Li, S., & Guo, Z. (2020). Comparisons of Heuristic, General Statistical and Machine Learning Models for Landslide Susceptibility Prediction and Mapping. *Catena*, 191(104580), 1–14. doi: 10.1016/j.catena.2020.104580

Hussain, M. A., Chen, Z., Wang, R., Shah, S. U., Shoaib, M., Ali, N., Xu, D., & Ma, C. (2022). Landslide Susceptibility Mapping Using Machine Learning Algorithm. *Civil Engineering Journal*, 8(2), 209–224. https://doi.org/10.28991/CEJ-2022-08-02-02

Hussain, M. A., Chen, Z., Zheng, Y., Zhou, Y., & Daud, H. (2023). Deep Learning and Machine Learning Models for Landslide Susceptibility Mapping with Remote Sensing Data. *Remote Sensing*, 15(19), 1–30. doi: 10.3390/rs15194703

Hussain, M. A., Chen, Z., Zhou, Y., Meena, S. R., Ali, N., & Shah, S. U. (2025). Landslide Susceptibility Mapping Using Artificial Intelligence Models: A Case study in The Himalayas. *Landslides*, 22(6), 2089–2103. doi: 10.1007/s10346-025-02466-2

James, G., Witten, D., Hastie, T., & Tibshirani, R. (2013). *An Introduction to Statistical Learning with Applications R*. Springer.

Kavzoglu, T., & Teke, A. (2022). Predictive Performances of Ensemble Machine Learning Algorithms in Landslide Susceptibility Mapping Using Random Forest, Extreme Gradient Boosting (XGBoost) and Natural Gradient Boosting (NGBoost). *Arabian Journal for Science and Engineering*, 47, 7367–7385. https://doi.org/10.1007/s13369-022-06560-8

Khadka, D., Zhang, J., & Sharma, A. (2025). Geographic Object-Based Image Analysis for Landslide Identification Using Machine Learning on Google Earth Engine. *Environmental Earth Sciences*, 84(92), 1–27. doi: 10.1007/s12665-024-12045-8

Khan, M. Y., Qayoom, A., Nizami, M. S., Siddiqui, M. S., Wasi, S., & Raazi, S. M. K. (2021). Automated Prediction of Good Dictionary EXamples (GDEX): A Comprehensive Experiment with Distant Supervision, Machine Learning, and Word Embedding-Based Deep Learning Techniques. *Complexity*, *2021*, 1–18.

Landis, J. R., & Koch, G. G. (1977). Measurement of Observer Agreement for Categorical Data. *Biometrics*, 33, 159–174. doi: 10.2307/2529310

Le, X. H., Choi, C., Eu, S., Yeon, M., & Lee, G. (2024). Quantitative Evaluation of Uncertainty and Interpretability inMachine Learning-Based Landslide Susceptibility Mapping Through Feature Selection and Explainable AI. *Frontiers in Environmental Science*, *12*, 1–15. https://doi.org/10.3389/fenvs.2024.1424988

Li, H., Liu, Q., Wang, Z., Huang, F., Chen, X., Hu, H., Gu, H., Hu, W., & Zhou, X. (2025). Regional Landslide Susceptibility Prediction Considering The Optimal Discretization of Environmental Factors. *Geocarto International*, 40(1), 1–24. doi: 10.1080/10106049.2025.2543487

Liang, Z., Peng, W., Liu, W., Huang, H., Huang, J., Lou, K., Liu, G., & Jiang, K. (2023). Exploration and Comparison of the Effect of Conventional and Advanced Modeling Algorithms on Landslide Susceptibility Prediction: A Case Study from Yadong Country, Tibet. *Applied Sciences*, 13(12), 1–20. doi: 10.3390/app13127276

Liu, L. (2024). An Ensemble Framework for Explainable Geospatial Machine Learning Models. *International Journal of Applied Earth Observation and Geoinformation*, 132(36), 1–12. doi: 10.1016/j.jag.2024.104036

Liu, Q., Tang, A., Huang, Z., Sun, L., & Han, X. (2022). Discussion on The Tree-Based Machine Learning Model in The Study of Landslide Susceptibility. *Natural Hazards*, 113(2), 887–911. doi: 10.1007/s11069-022-05329-4

Meena, S. R., Hussain, M. A., Ullah, H., & Ullah, I. (2025). Landslide Susceptibility Mapping Using Hybrid Machine Learning Classifiers: A Case Study of Neelum Valley, Pakistan. *Bulletin of Engineering Geology and the Environment*, 84(242), 1–20. doi: 10.1007/s10064-025-04270-7

Melati, D. N., Umbara, R. P., Astisiasari, A., Wisyanto, W., Trisnafiah, S., Trinugroho, T., Prawiradisastra, F., Arifianti, Y., Ramdhani, T. I., Arifin, S., & Anggreainy, M. S. (2024). A Comparative Evaluation of Landslide Susceptibility Mapping Using Machine Learning-Based Methods in Bogor Area of Indonesia. *Environmental Earth Sciences*, 83(3), 1–42. doi: 10.1007/s12665-023-11402-3

Muhardi, & Perdhana, R. (2025). Soil Magnetic Susceptibility Analysis as an Indicator of Landslide-Prone Areas in Sanggau Regency, West Kalimantan Province, Indonesia. *Journal of Degraded and Mining Lands Management*, 12(2), 7185–7195. doi: 10.15243/jdmlm.2025.122.7185

Noviari, S., Salfira, G., Raudhah, A. F., Haerudin, N., & Mulyasari, R. (2023). Mitigasi Daerah Rawan Bencana Longsor di Kota Batu dengan Menggunakan Metode Analisis SIG. *Journal of Applied Geoscience and Engineering*, 2(2), 57–65. doi: 10.37905/jage.v2i2.20753

Noviyanto, A., Sartohadi, J., & Purwanto, B. H. (2020). The Distribution of Soil Morphological Characteristics for Landslide-Impacted Sumbing Volcano, Central Java-Indonesia. *Geoenvironmental Disasters*, 7(25), 1–19. doi: 10.1186/s40677-020-00158-8

Nurwatik, N., Ummah, M. H., Cahyono, A. B., Darminto, M. R., & Hong, J. H. (2022). A Comparison Study of Landslide Susceptibility Spatial Modeling Using Machine Learning. *ISPRS International Journal of Geo-Information*, 11(12), 1–21. doi: 10.3390/ijgi11120602

Pappaka, R. K., Nakkala, A. B., Badapalli, P. K., Gugulothu, S., Anguluri, R., Hasher, F. F. Ben, & Zhran, M. (2025). Machine Learning-Driven Groundwater Potential Zoning Using Geospatial Analytics and Random Forest in the Pandameru River Basin, South India. *Sustainability*, 17(9), 1–25. doi: 10.3390/su17093851

Pasang, S., & Kubíček, P. (2020). Landslide Susceptibility Mapping Using Statistical Methods Along the Asian Highway, Bhutan. *Geosciences*, *10*(11), 1–26. doi: 10.3390/geosciences10110430

Prasetyo, S. T., Rahman, F. A., Suryawati, S., Supriyadi, S., & Setiawan, E. (2025). Land Use Analysis Using Machine-Learning Based on Cloud Computing Platform. *Indonesian Journal of Agricultural Sciences*, 30(4), 765–772. doi: 10.18343/jipi.30.4.765

Pratiwi, E. S., Shen, S., & Sartohadi, J. (2024). Understanding the Nature of Landslides Through Detailed Geomorphological Mapping on The Sumbing Volcanic Landscape, Java Island, Indonesia. *Journal of Maps*, 20(1), 1–13. doi: 10.1080/17445647.2024.2429710

Qi, T., Meng, X., & Zhao, Y. (2024). Landslide Susceptibility Assessment in Active Tectonic Areas Using Machine Learning Algorithms. *Remote Sensing*, 16(15), 1–16. doi: 10.3390/rs16152724

Qi, T., Zhao, Y., Meng, X., Shi, W., Qing, F., Chen, G., Zhang, Y., Yue, D., & Guo, F. (2021). Distribution Modeling and Factor Correlation Analysis of Landslides in the Large Fault Zone of the Western Qinling Mountains: A Machine Learning Algorithm. *Remote Sensing*, 13(4990), 1–24. doi: 10.3390/rs13244990

Qiu, A., Wang, Q., Chen, Y., Tao, K., Peng, X., He, W., Gao, L., Geli, O., & Zhang, F. (2024). Landslide Susceptibility Assessment in Hong Kong with Consideration of Spatio-Temporal Consistency. *Applied Sciences*, 14(22), 1–20. doi: 10.3390/app142210654

Susilo, A., Juwono, A. M., Aprilia, F., Hisyam, F., Rohmah, S., & Hasan, M. F. R. (2023). Subsurface Analysis Using Microtremor and Resistivity to Determine Soil Vulnerability and Discovery of New Local Fault. *Civil Engineering Journal*, 9(9), 2286–2299. doi: 10.28991/CEJ-2023-09-09-014

Suwarno, S., Rachmawati, E., Ibrahim, M. H., Sutomo, S., & Slamet, A. (2025). Analysis of Spatial Planning in Landslide Hazard Zones in Banyumas Regency, Indonesia. *Forum Geografi*, 39(1), 79–88. doi: 10.23917/forgeo.v39i1.6685

Tao, H., Salih, S., Oudah, A. Y., Abba, S. I., Ameen, A. M. S., Awadh, S. M., Yaseen, O. A. A., Mostafa1, R. R., Surendran, U. P., & Yaseen, Z. M. (2022). Development of New Computational Machine Learning Models for Longitudinal Dispersion Coefficient Determination: Case Study of Natural Streams, United States. *Environmental Science and Pollution Research*, 29(24), 35841–35861. doi: 10.1007/s11356-022-18554-y

Tjahjono, B., Firdania, I., & Trisasongko, B. H. (2024). Modeling Landslide Hazard Using Machine Learning: A Case Study of Bogor, Indonesia. *Journal of Natural Resources and Environmental Management*, 14(2), 407–414. doi: 10.29244/jpsl.14.2.407

Ullah, K., Wang, Y., Li, P., Fang, Z., Rahaman, M., Ullah, S., & Hamed, M. M. (2024). Spatiotemporal Dynamics of Landslide Susceptibility Under Future Climate Change and Land Use Scenarios. *Environmental Research Letters*, *19*(124016), 1–17. doi: 10.1088/1748-9326/ad8a72

Wu, W., Zhang, Q., Singh, V. P., Wang, G., Zhao, J., Shen, Z., & Sun, S. (2022). A Data-Driven Model on Google Earth Engine for Landslide Susceptibility Assessment in the Hengduan Mountains, the Qinghai-Tibetan Plateau. *Remote Sensing*, 14(18), 1–24. doi: 10.3390/rs14184662

Xu, S., Song, Y., & Hao, X. (2022). A Comparative Study of Shallow Machine Learning Models and Deep Learning Models for Landslide Susceptibility Assessment Based on Imbalanced Data. *Forests*, 13(11), 1–32. doi: 10.3390/f13111908

Zeng, Y., Zhang, Y., Hu, W., Chen, M., Hu, Q., Liu, X., & Zhu, X. (2024). A Case Study on Soil Slope Landslide Failure and Parameter Analysis of Influencing Factors for Safety Factor Based on Strength Reduction Method and Orthogonal Experimental Design. *Plos One*, 19(5), 1–20. doi: 10.1371/journal.pone.0300586

Zhou, C., Wang, Y., Cao, Y., Singh, R. P., Ahmed, B., Motagh, M., Wang, Y., Chen, L., Tan, G., & Li, S. (2024). Enhancing Landslide Susceptibility Modelling Through a Novel Non-Landslide Sampling Method and Ensemble Learning Technique. *Geocarto International*, 39(1), 1–25. doi: 10.1080/10106049.2024.2327463